

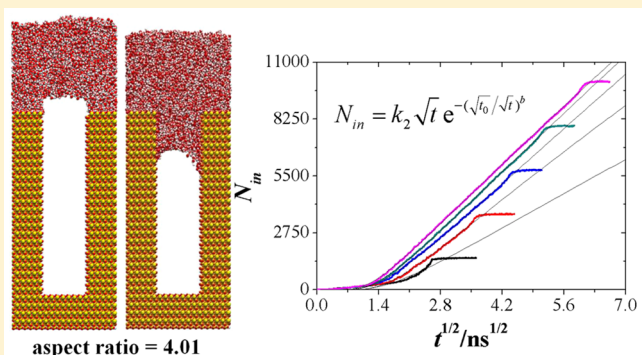
# Effects of Aspect Ratio on Water Immersion into Deep Silica Nanoholes

Jing Zheng,<sup>†</sup> Junqiao Zhang,<sup>†</sup> Lu Tan,<sup>†</sup> Debing Li,<sup>†</sup> Liangliang Huang,<sup>‡</sup> Qi Wang,<sup>\*,†</sup> and Yingchun Liu<sup>\*,†</sup>

<sup>†</sup>Department of Chemistry and Soft Matter Research Center, Zhejiang University, Hangzhou 310027, People's Republic of China

<sup>‡</sup>School of Chemical, Biological & Materials Engineering, University of Oklahoma, Norman, Oklahoma 73019, United States

**ABSTRACT:** Understanding the influence of aspect ratio on water immersion into silica nanoholes is of significant importance to the etching process of semiconductor fabrication and other water immersion-related physical and biological processes. In this work, the processes of water immersion into silica nanoholes with different height/width aspect ratios ( $\phi = 0.87, 1.92, 2.97, 4.01, 5.06$ ) and different numbers of water molecules ( $N = 9986, 19972, 29958, 39944$ ) were studied by molecular dynamics simulations. A comprehensive analysis has been conducted about the detailed process of water immersion and the influence of aspect ratios on water immersion rates. Five distinguishable stages were identified for the immersion process with all studied models. The results reveal that water can easily immerse into the silica nanoholes with larger  $\phi$  and smaller  $N$ . The calculation also suggests that aspect ratios have a greater effect on water immersion rates for larger  $N$  numbers. The mechanism of the water immersion process is discussed in this work. We also propose a mathematical model to correlate the complete water immersion process for different aspect ratios.



## INTRODUCTION

How the process of water immersion into silica nanoholes is affected by the height/width aspect ratio is of practical importance to the etching of semiconductor fabrication, especially when the size of integrated circuits is around a few nanometers.<sup>1,2</sup> Water immersion is also connected with biological, physical, and geological applications.<sup>3–5</sup> In the past two decades, theoretical studies of silica and water system have been focused on two aspects: interfacial water on silica surfaces<sup>6–14</sup> and confined water in silica nanopores.<sup>3–5,15–18</sup> Important results include, for instance, Adeagbo and coworkers applying Car–Parrinello molecular dynamics (MD) simulations and investigating the transport and dissolution processes at the  $\alpha$ -quartz/water interface under high temperatures and pressures.<sup>12</sup> They observed  $H_2O$  dissociation at the Si-terminated surface, which leads to a full surface hydroxylation in a very short time. Wensink et al. performed MD simulations to study the nature of adsorbed water and its effect on the interaction between two silica surfaces.<sup>14</sup> They observed the spontaneous formation of water bridge between two silica surfaces when their distance is  $<3$  nm. Steefel and coworkers performed MD simulations to study water confined in different silica nanopores (diameter: 1, 2, and 4 nm).<sup>3</sup> They discussed both confined water behavior (1 nm pore) and distinguishable water layers in the other two relatively larger pores, which also occurred for interfacial water.<sup>9,10,13,14</sup> It is important to note that most studies focus on the equilibrium structural properties of water; little has been discussed on how water immerses silica nanopores and what are the important factors for such processes.

Mechanisms of liquids into porous materials with different diameters have been studied both theoretically<sup>5,19–26</sup> and experimentally.<sup>27–30</sup> Spontaneous uptake of liquid water, which is driven by capillary forces, is one of the proposed water immersion mechanisms. Gruener et al. performed experiments on the capillary rise of water into hydrophilic silica pores (Vycor monoliths) with different pore radius (3.4 and 4.9 nm) in the 3-D networks.<sup>27</sup> Porous materials in these studies are connected to the liquid reservoir. They concluded that the imbibition dynamics during the entire capillary rise was consistent with the Lucas–Washburn laws. However, the water immersion mechanism remains unknown when exposed to the realistic humid conditions. Yamashita et al. performed NVT MD simulations on water uptake into a fully hydroxylated silica nanopore with 1.38 nm pore radius and 7.93 nm film thickness.<sup>5</sup> In their calculation, different numbers of water molecules were tested, and the results suggested that the water transport mechanism depends on the number of water molecules. It is worth noting that in their calculation the initial quick flow can be described by Lucas–Washburn laws, and the sequentially slow process agrees with the Fickian diffusion theory.<sup>5</sup>

Despite the progress, the water immersion mechanism into nanoholes is still not clear. For example, what is the correlation of water immersion process and nanoholes height/width aspect ratio? Is water number (density) an important factor for

Received: April 25, 2016

Revised: July 3, 2016

Published: August 9, 2016

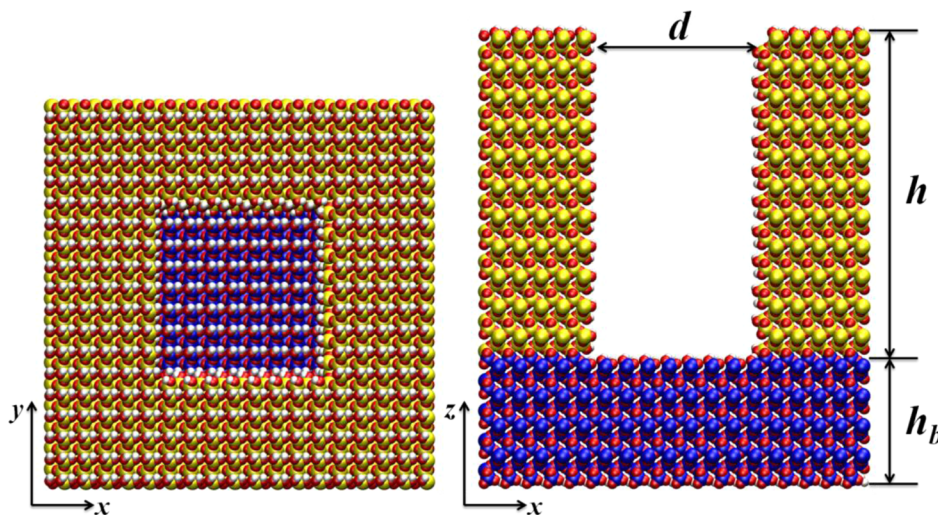


**Figure 1.** Top (left) and cross-sectional view (right) of starting structure of the silica nanohole for  $\phi = 1.92$ .  $\phi$  was defined as  $h/d$ , where  $d$  was 3.9824 nm for all models. For the base with  $h_b$  height, blue spheres represented Si atoms, while yellow spheres represented Si atoms for the above. Red and white spheres represented O and H atoms, respectively.

determining the immersion process? Because it is known that the immersion involves different stages, is there a model or sequential models to capture the complete process? To shed light on those fundamental questions, we adopted simple silica nanoholes models and applied MD simulations to study the water immersion process. A series of silica nanoholes with various aspect ratios ( $\phi = 0.87, 1.92, 2.97, 4.01, 5.06$ ), defined as the ratio between the depth and the width of the nanoholes, were constructed. Different numbers of water molecules ( $N = 9986, 19972, 29958, 39944$ ) were placed on the surface of nanoholes with an initial water/nanoholes distance of 0.4 nm. The results are discussed in terms of both the structural and kinetic properties of water in the nanoholes and how they are affected by the aspect ratio ( $\phi$ ) and the number of water molecules ( $N$ ).

## SIMULATION METHODS

**Silica Nanohole Models.** To construct a series of silica nanoholes with various aspect ratios, we chose cristobalite, a regular crystal lattice, as our model material. The dimension of the unit cell was 0.4978 (width,  $x$ )  $\times$  0.4978 (length,  $y$ )  $\times$  0.6948 (height,  $z$ ) nm<sup>3</sup>, where we defined  $d_0 = 0.4978$  nm and  $h_0 = 0.6948$  nm. Illustrated by the  $\phi = 5.06$  model, all models were constructed by the following steps: (I) The unit cell was expanded to the  $18 \times 18 \times 33$  supercell (consists of 10 692 unit cells), of which the volume was  $8.9604 \times 8.9604 \times 22.9284$  nm<sup>3</sup>. (II) The supercell was then cleaved along the (001) direction to create a slab model via the Materials Studio software.<sup>31</sup> The cleaved surfaces were defined as the slab surfaces. (III) The  $8 \times 8 \times 29$  cell (consists of 1856 unit cells), which was located at the center of the  $x-y$  plane, location defined by  $4h_0 < z < 33h_0$ , was removed from the slab to form the nanoholes model used in the calculation. The width of the nanohole ( $d$ ) was 3.9824 nm ( $8d_0$ ) and the height of the base ( $h_b$ ) was  $4h_0$ . The height of the nanohole ( $h$ ) was about  $29h_0$  (which was  $5h_0, 11h_0, 17h_0$ , and  $23h_0$  for other nanoholes, where  $\phi = 0.87, 1.92, 2.97, 4.01$ ). (IV) The O atoms were removed if covalently bound to fewer than one Si atom. The Si atoms coordinated to fewer than two O atoms were also removed. The dangling Si atoms were saturated by OH groups. H atoms were attached to each singly coordinated O atom in both the slab and the hole surfaces. (V) The as-constructed system was finally energy minimized as the final silica nanohole models with different aspect ratios. It is worth noting that there were two different surface functional groups: the vicinal silanol groups (Si atoms bonded with only one hydroxyl group) in the (100, 010) hole surfaces and the geminal silanol groups (Si atoms bonded with two hydroxyl groups) in the (001) surfaces. In this study, the number densities of silanol groups in the (100, 010) hole surfaces and the (001)

slab surfaces are 5.8 and 8.0 OH nm<sup>-2</sup>, respectively. They are smaller than the values (7.2 and 9.6 OH nm<sup>-2</sup>, respectively) reported by Yamashita et al.<sup>5,6</sup> This is due to the different forms of the crystal used in this work. The average density of silanol groups in our models is consistent with the value ( $6.6 \pm 0.2$  OH nm<sup>-2</sup>) reported by Bourg and coworkers.<sup>3</sup> Different values, from 6.8 to 7.6 OH nm<sup>-2</sup> have been also reported from various interatomic potential models.<sup>4,17,32</sup> For example, for silica surfaces, the value was reported to be 4.9 OH nm<sup>-2</sup>.<sup>33</sup> Here the discrepancy is from different definitions of surface area: Zhuravlev adopted the effective surface area measured by the low-temperature adsorption of Kr, while an ideal surface area, which is derived as if the surface is smooth, is used in our study.

Larger aspect ratios represent larger vacuum volumes of the nanoholes in silico. The number of air molecules that the nanoholes could contain in standard atmospheric pressure at 300 K was calculated to examine the reliability of our models, and it was found that the nanoholes were almost vacuum. It is also worth adding that the dimension of our silica models was almost the same as the targeted size of SiO<sub>2</sub> films in the integrated circuits projected for next decade. Bulk water with different thicknesses, 3.7241 nm (for  $N = 9986$ ), 7.4482 nm (for  $N = 19972$ ), 11.1723 nm (for  $N = 29958$ ), and 14.8964 nm (for  $N = 39944$ ), was placed on the surface of each nanohole model, with an initial water/nanohole distance of 0.4 nm. A 10 nm thick vapor gap was set above the bulk water in the  $z$  direction in all models. Figure 1 demonstrates the initial structure of a silica nanohole,  $\phi = 1.92$ .

**Simulation Details.** In this study, MD simulations with different numbers of water at different nanoholes were carried out with the GROMACS (GROningen MACHine for Chemical Simulations) software package.<sup>34</sup> Parameters for silica were derived from ref 14. Internal atoms were frozen in space and only the atoms at the surfaces were allowed to move to avoid unnecessary structural changes. For water, the SPC/E (extended simple point charge) water model was adopted.<sup>35</sup> The 3-D periodic boundary condition was employed. The geometry of silanol groups and water molecules were constrained by the LINCS algorithm.<sup>36</sup> All simulations were implemented in the NVT ensemble at 300 K with a 2 fs time step. Leap-frog algorithm was employed to integrate the equation of motion for the system.<sup>37</sup> The system temperature was controlled by a Velocity rescaling thermostat (a modified Berendsen thermostat).<sup>38</sup> The cutoff radius for both the Lennard-Jones (6–12) potential and long-range Coulombic interaction was 1.2 nm. The long-range Coulombic interactions were calculated by the particle mesh Ewald (PME) method.<sup>39,40</sup> NVT MD simulations were carried out, and it was considered that the equilibrium has been achieved when the number of water immersion molecules ( $N_{in}$ ) remained constant and the center-of-mass of water molecules remained stable along the  $z$  direction for several nanoseconds.

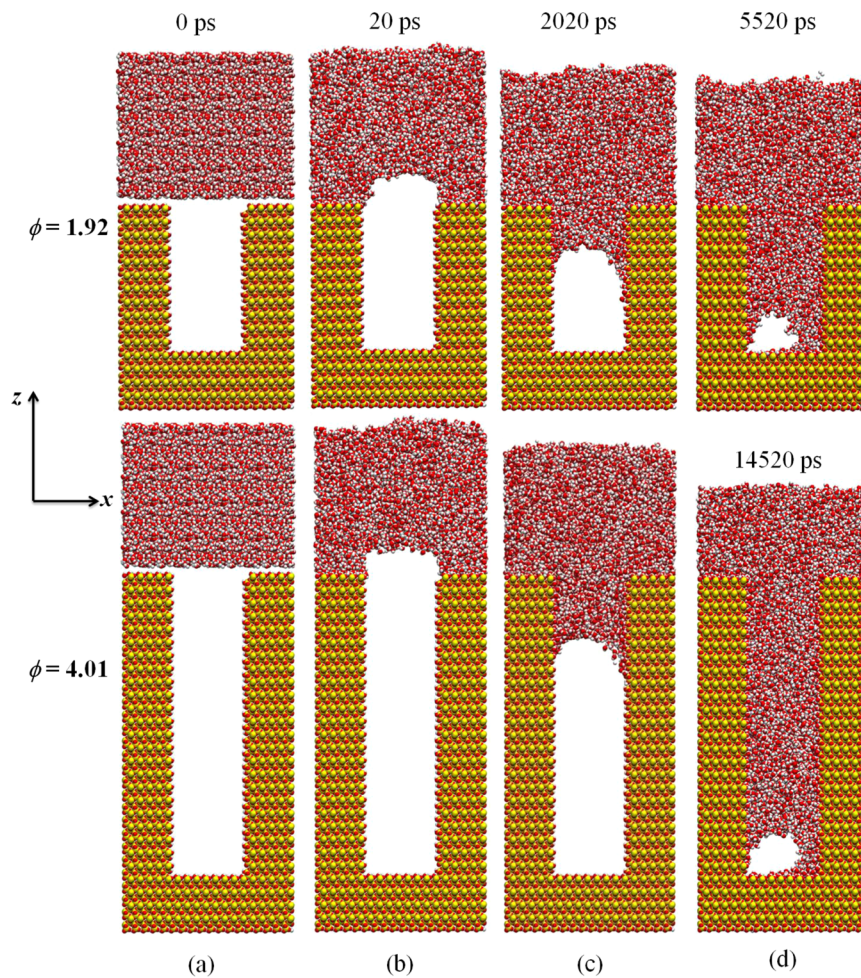


**Figure 2.** Snapshots of water immersion for  $N = 19\,972$ ,  $\phi = 1.92$  (top) and  $N = 19\,972$ ,  $\phi = 4.01$  (below) at 300 K along the time (yellow, red, and white: Si, O, and H atoms, respectively): (a) 0, (b) 20, (c) 2020, and (d) 5520 ps for  $\phi = 1.92$  and 14 520 ps for  $\phi = 4.01$ .

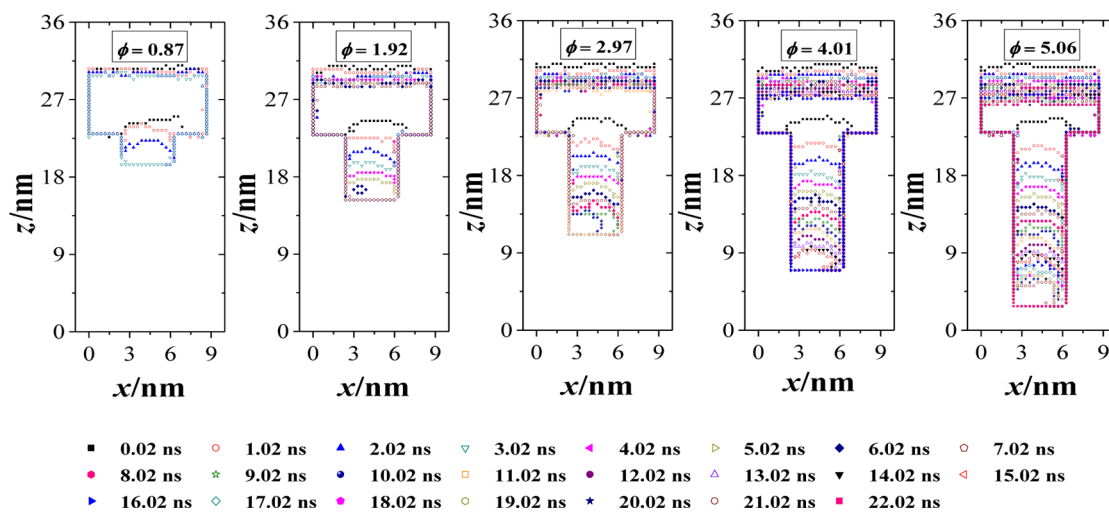


**Figure 3.** Time evolution of vapor/silica-liquid interface profiles for the bulk water ( $N = 19972$ ) in the systems of  $\phi = 0.87, 1.92, 2.97, 4.01, 5.06$  at 300 K.

## RESULTS AND DISCUSSION

**Process Analysis of Water Immersion with Different Aspect Ratios.** Snapshots of water immersion into silica nanoholes along time for  $N = 19\,972$ ,  $\phi = 1.92$  and  $N = 19\,972$ ,  $\phi = 4.01$  are displayed in Figure 2. Capillary rise occurred over time in both situations.

To describe the detailed process of water immersion, we calculated the profiles of vapor/silica–liquid interface from the number density profiles of the O atoms in water molecules (OW). Considering the symmetry of  $x$ – $y$  directions, the vapor/silica-liquid interface profiles were plotted in the  $x$ – $z$  plane. 30 visual slices were used in the  $x$  direction, while 61, 71, 82, 92, 103 visual slices were partitioned in the  $z$  direction for  $\phi = 0.87, 1.92,$

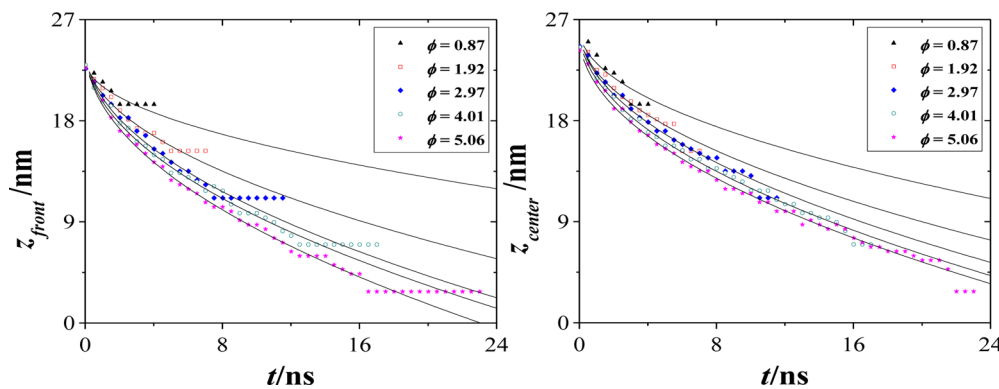


**Figure 4.**  $z$  position of the front ( $z_{\text{front}}$ , left) and the center ( $z_{\text{center}}$ , right) of water meniscus as a function of time at 300 K.  $z_{\text{center}}$  was defined as the  $z$  value of the middle position of water meniscus. The data were fitted by eq 1 except horizontal segments.

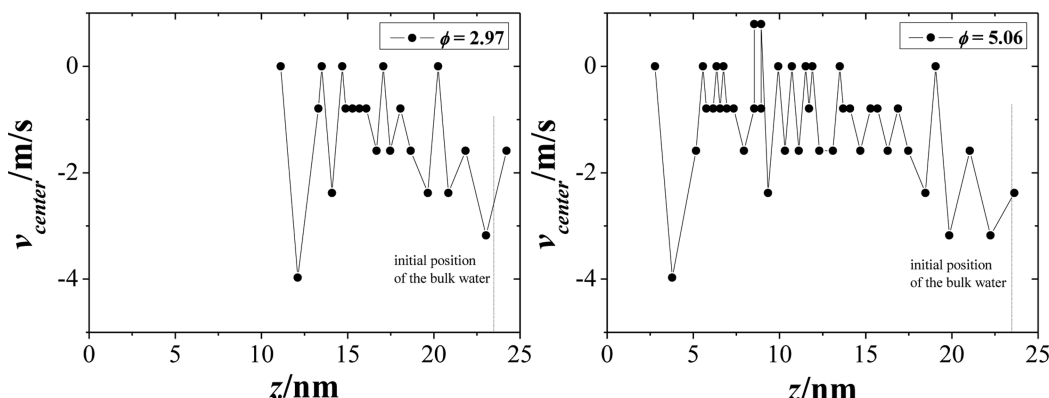


**Figure 5.** Velocity of the center of water meniscus along the  $z$  axis for  $\phi = 2.97$  and 5.06 at 300 K. The short dotted line represented the initial position where the bulk water was placed. The minus indicates that the direction of the motion was along the opposite direction of the  $z$  axis.

2.97, 4.01, and 5.06, respectively, to analyze the data accurately. The width and the height of each slice were 0.3 and 0.4 nm. The bulk water in the center of the  $y$  direction was selected to average the number density. The number of OW in each slice was calculated, and the vapor/silica–liquid interface profiles were derived from the peripheries of 2-D number density profiles. Figure 3 showed the vapor/silica–liquid interface profiles for  $N = 19972$  in the systems of  $\phi = 0.87$ , 1.92, 2.97, 4.01, and 5.06 as a function of simulation time. The process of water immersion could be clearly divided into five stages: (I) slow approaching the entrance of the nanohole (corresponding to snapshot (b) in Figure 2); (II) fast immersing the nanohole (corresponding to snapshot (c) in Figure 2); (III) slow moving to wet the nanohole (similar to snapshot (c)); (IV) slow wetting the bottom of the nanohole (corresponding to snapshot (d) in Figure 2); and (V) full filling the nanohole. Figure 4 further supports the five distinct stages by demonstrating the  $z$  position of the front ( $z_{\text{front}}$ ) and the center ( $z_{\text{center}}$ ) of water meniscus as a function of time.

In Stage I, the water molecules near the slab surface were quickly adsorbed onto it, while the water molecules near the entrance of the nanohole slightly moved backward to the bulk water, forming a meniscus at the entrance. Such process is also obvious when comparing the  $z_{\text{front}}$  with  $z_{\text{center}}$  at the beginning in Figure 4. In all five studied systems, the bulk water was initially placed at  $z_0 = 23.45$  nm. At the beginning,  $z_{\text{center}}$  was greater than  $z_0$  and even larger than 24 nm for  $\phi < 2$ , while  $z_{\text{front}}$  was smaller than  $z_0$  and nearly the same. This indicates that aspect ratios do not affect the  $z_{\text{front}}$  and the front comes to the surface quickly, while they affect the  $z_{\text{center}}$  and the center moves back toward the

bulk water more with decreasing aspect ratios. We noted this phenomenon as hysteresis. It is the hysteresis that determines the center approach to the entrance of the nanohole a slow process. The hysteresis is obvious and is more stable with lower aspect ratios. In Stage II, the bulk water molecules immersed into the silica nanoholes fast with a meniscus at the front. This was owing to the OH groups of the hole surfaces. The bulk water immersed deeper at the same time intervals as the aspect ratios increased, which was also shown in Figure 4. In Stage III, the rate of water immersion declined when the bulk water came to a certain depth of the nanohole. The bulk water came down along the hole wall faster than that in the center of the nanohole, so the curvature of the meniscus slightly increased. Such stage was not obvious at low aspect ratios. In Stage IV, when approaching to the bottom of the nanohole, water molecules first wet the bottom along the surface, which may be due to the higher OH group density of the bottom surface ([001]). It was a good illustration that the  $z_{\text{front}}$  kept constant in last several nanoseconds. A spherical vacuum was formed in the bulk water near the bottom when the hole surfaces were completely wetted. In Stage V, the spherical vacuum was fulfilled with water rapidly once formed, which was also supported in Figure 4, where the  $z_{\text{center}}$  suddenly decreased before remaining constant. For  $\phi < 3$ , the last three stages were not obvious in Figure 3, which was largely because these three stages finished in short time at low aspect ratios. After these five stages, the silica nanoholes with different aspect ratios were all fulfilled with water. Figures 3 and 4 indicate that higher aspect ratios are more beneficial for Stages I and II but not better for Stages III and IV of water immersion, which was further

supported by Figure 5. Figure 5 showed the velocity of the center of water meniscus along the  $z$  axis for  $\phi = 2.97$  and 5.06. The minus represented that the direction of the motion was along the opposite direction of the  $z$  axis. The distribution of the velocity for two aspect ratios could be roughly divided into three areas: initial rapid area (including Stages I and II), middle slow area (including Stages III and IV), and final fast area (Stage V). It was clearly seen that the velocity for  $\phi = 2.97$  was lower than that for  $\phi = 5.06$  in the initial rapid area. The length of this area for two aspect ratios was nearly the same, while the length of the middle slow area for  $\phi = 5.06$  was much longer than that for  $\phi = 2.97$ , which indicates that increasing aspect ratios extends the length of the middle slow area. The velocity for  $\phi = 5.06$  in the middle slow area included many zeros and even appeared as a positive value, which indicated that the center of the water meniscus kept still or even moved back toward the bulk water. The velocity of the final fast area was basically the same, which indicates that aspect ratios do not affect this area.

It has been reported by Yamashita<sup>5</sup> that the bulk water moved into the silica nanopore as a water column when it came to a certain number of water molecules. They also showed that the water column moved downward, with a water meniscus formed at the front, as our Stages II and III. Stages I, IV, and V were not shown in their water uptake process. This difference may be owing to the following two reasons: the numbers of water molecules are much larger than those in their study and our models are nanoholes while theirs are nanopores.

Furthermore, the data in Figure 4 were fitted by the Lucas–Washburn law.<sup>5,21,27,41</sup> The Lucas–Washburn law describes capillary flow in a bundle of parallel cylindrical tubes and could be extended to imbibition into porous materials. In our study, the Lucas–Washburn law could be used to describe time evolution of the length of water column. According to the Lucas–Washburn law, the length of the water column was proportional to  $t^{0.5}$ . Figure 4 was fitted by the following equation

$$z - z_i = -\sqrt{kt} \quad (1)$$

where  $z_i$  and  $k$  were fitting parameters and  $k$  was the function of surface tension, viscosity, and the dimension of the nanohole. All fitted curves are shown in Figure 4. The fitted results are summarized in Table 1.

From the fitted curves and the value of  $R^2$ , it could be seen that the data were well fitted by the equation except  $\phi = 0.87$ . This suggests that aspect ratios should not influence the transport mechanism, which is the transport of water columns. Table 1 also

**Table 1. Fitting Ranges and Fitted Parameters for Water Immersion in Different Aspect Ratios<sup>a</sup>**

$z_{\text{front}} - t$	[ $t_{\text{start}}, t_{\text{end}}$ ]/ns	$z_i/\text{nm}$	$k/\text{nm}^2/\text{ns}$	$R^2$
$\phi = 0.87$	[0, 2.02]	23.40	5.46	0.7891
$\phi = 1.92$	[0, 5.02]	24.16	14.17	0.9698
$\phi = 2.97$	[0, 7.52]	24.61	20.86	0.9716
$\phi = 4.01$	[0, 12.52]	24.44	22.29	0.9913
$\phi = 5.06$	[0, 16.52]	24.51	26.06	0.9945
$z_{\text{center}} - t$	[ $t_{\text{start}}, t_{\text{end}}$ ]/ns	$z_i/\text{nm}$	$k/\text{nm}^2/\text{ns}$	$R^2$
$\phi = 0.87$	[0, 3.02]	26.21	9.56	0.7292
$\phi = 1.92$	[0, 6.02]	26.20	14.79	0.9413
$\phi = 2.97$	[0, 10.52]	26.41	18.43	0.9823
$\phi = 4.01$	[0, 16.02]	26.16	20.09	0.9931
$\phi = 5.06$	[0, 22.02]	25.69	20.56	0.9938

<sup>a</sup> $R^2$  is corrected determination coefficient for the fitted curves.

showed that the value of  $k$  for  $z_{\text{front}} - t$  ( $z_{\text{center}} - t$ ) curves increased from 5.46 (9.56)  $\text{nm}^2/\text{ns}$  to 26.06 (20.56)  $\text{nm}^2/\text{ns}$  as aspect ratios increased, which indicates that water immersion is easier for silica nanoholes with higher aspect ratios. The increments of  $k$  for  $z_{\text{center}} - t$  curves between two adjacent aspect ratios decreased from 5.23 to 0.47  $\text{nm}^2/\text{ns}$  as aspect ratios increased, which indicates that the change of aspect ratios has a more significant impact on water immersion at low aspect ratios.

**Water Immersion Curves.** To better compare the effects of different aspect ratios on water immersion, we calculated the number of water molecules located in each nanohole,  $N_{\text{in}}$ , at each frame of the trajectory. To avoid the influence of the pore inlet, we defined the threshold value of  $z$  as 22.58 nm. That is to say,  $N_{\text{in}}$  was the number of water molecules within  $z < 22.58$  nm. Figure 6 shows the time evolution of  $N_{\text{in}}$  for different aspect ratios at each number of water molecules, which is called the water immersion curve in this paper. It is clearly shown that the hysteresis in Stage I enhanced with decreasing  $\phi$  and increasing  $N$ , which indicates that high  $\phi$  and small  $N$  make water immersion easier at the entrance of the nanoholes. At the beginning, the difference in  $N_{\text{in}}$  for two adjacent water immersion curves was small for  $\phi > 3$  but distinct for  $\phi < 3$ , which was more evident for large  $N$ . This indicates that aspect ratios have a significant effect on water immersion at the entrance within small  $\phi$  and large  $N$ . Then, the differences all increased first and then decreased along time, which is due to high aspect ratios being beneficial for Stages I and II but not good for Stages III and IV. For each system of the same  $N$ , it could be seen that  $N_{\text{in}}$  was larger at the same time as aspect ratios increased, which indicates that water molecules immerse into silica nanoholes with high aspect ratios more quickly.

Yamashita et al.<sup>5</sup> reported that the capillary rise expressed by the Lucas–Washburn Law was the dominant mechanism when the water molecules above the surface were enough to fully fill the nanopore. Because water molecules were all enough in our study, the  $N_{\text{in}} - t$  curves were all fitted by the function below

$$N_{\text{in}} - N_{\text{in},0} = \sqrt{k_1 t} \quad (2)$$

where  $N_{\text{in},0}$  and  $k_1$  are the two fitting parameters. Because of the different numbers of water molecules ( $\Delta N$ ) needed to fill in the diverse nanoholes, the left of eq 2 was not divided by  $\Delta N$  like Yamashita et al.<sup>5</sup>  $\Delta N$  was included in  $k_1$ , so  $k_1$  was the function of the dimension of the nanohole, surface tension, and viscosity. Here  $k_1$  could indicate the water immersion rates for the whole process. The fitted curves are shown in Figure 6 and the fitted results are summarized in Table 2. From the fitted curves and the value of  $R^2$ , it could be seen that the water immersion curves were not well-fitted for  $\phi = 0.87$  and 1.92,  $N > 2000$ . This is due to the strong hysteresis in Stage I. The value of  $k_1$  increased as the aspect ratios increased at each  $N$ , but the distinction of  $k_1$  for two adjacent water immersion curves decreased, for example, from  $2.47 \times 10^6$  to  $0.3 \times 10^6 \text{ ns}^{-1}$  for  $N = 19972$ . This indicates that water immersion rates increase with increasing  $\phi$  but the effect of aspect ratios on water immersion weakens. When  $\phi > 3$ , increasing aspect ratios will make little influence on water immersion. This result also implies that aspect ratios should make no difference in water immersion when reaching a certain value.

The dimensions of our silica nanoholes are relatively consistent with what is expected to study in practical application, while the number of water molecules in silico is difficult to reach at the macro level. This is why the effect of numbers of water

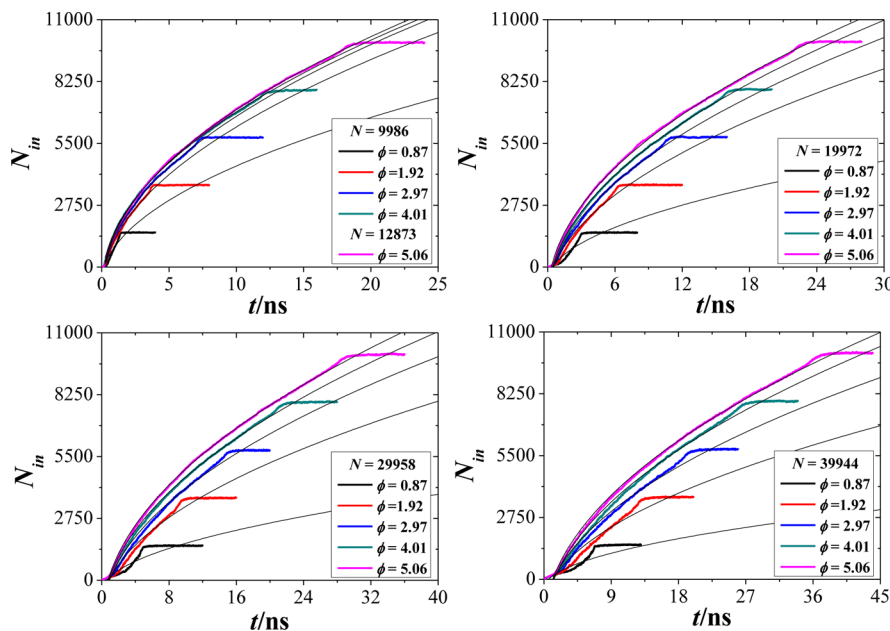


**Figure 6.** Time evolution of  $N_{in}$  for different aspect ratios at each number of water molecules at 300 K. The black solid curves showed the curves fitted by eq 2.

**Table 2. Fitting Ranges and Fitted Parameters for the Water Immersion Curves at Different  $\phi$  and  $N$  by Equation 2<sup>a</sup>**

$N = 9986$	$[t_{start}, t_{end}] / \text{ns}$	$N_{in\_0}$	$k_1 / \text{ns}^{-1}$	$R^2$
$\phi = 0.87$	[0, 1.41]	-717	$2.72 \times 10^6$	0.8825
$\phi = 1.92$	[0, 3.82]	-1006	$5.24 \times 10^6$	0.9900
$\phi = 2.97$	[0, 7.45]	-1008	$5.95 \times 10^6$	0.9979
$\phi = 4.01$	[0, 12.33]	-809	$5.94 \times 10^6$	0.9993
$N = 12\,873$	$[t_{start}, t_{end}] / \text{ns}$	$N_{in\_0}$	$k_1 / \text{ns}^{-1}$	$R^2$
$\phi = 5.06$	[0, 18.77]	-1100	$6.97 \times 10^6$	0.9995
$N = 19\,972$	$[t_{start}, t_{end}] / \text{ns}$	$N_{in\_0}$	$k_1 / \text{ns}^{-1}$	$R^2$
$\phi = 0.87$	[0, 3.04]	-629	$9.54 \times 10^5$	0.8078
$\phi = 1.92$	[0, 6.46]	-1339	$3.44 \times 10^6$	0.9657
$\phi = 2.97$	[0, 10.99]	-1499	$4.57 \times 10^6$	0.9917
$\phi = 4.01$	[0, 16.19]	-1483	$5.18 \times 10^6$	0.9974
$\phi = 5.06$	[0, 23.04]	-1326	$5.48 \times 10^6$	0.9988
$N = 29\,958$	$[t_{start}, t_{end}] / \text{ns}$	$N_{in\_0}$	$k_1 / \text{ns}^{-1}$	$R^2$
$\phi = 0.87$	[0, 5.00]	-530	$4.73 \times 10^5$	0.7829
$\phi = 1.92$	[0, 9.80]	-1395	$2.19 \times 10^6$	0.9465
$\phi = 2.97$	[0, 15.35]	-1777	$3.43 \times 10^6$	0.9815
$\phi = 4.01$	[0, 21.69]	-1856	$4.17 \times 10^6$	0.9938
$\phi = 5.06$	[0, 29.32]	-1854	$4.64 \times 10^6$	0.9974
$N = 39\,944$	$[t_{start}, t_{end}] / \text{ns}$	$N_{in\_0}$	$k_1 / \text{ns}^{-1}$	$R^2$
$\phi = 0.87$	[0, 6.82]	-406	$2.72 \times 10^5$	0.7999
$\phi = 1.92$	[0, 13.13]	-1329	$1.48 \times 10^6$	0.9329
$\phi = 2.97$	[0, 19.67]	-1804	$2.58 \times 10^6$	0.9759
$\phi = 4.01$	[0, 27.01]	-2159	$3.48 \times 10^6$	0.9877
$\phi = 5.06$	[0, 37.01]	-2121	$3.81 \times 10^6$	0.9956

<sup>a</sup> $R^2$  is corrected determination coefficient for the fitted curves.

molecules on water immersion is considered. It was clearly shown that the value of  $k_1$  decreased with increasing  $N$  at each  $\phi$ , for example, from  $(5.95 \pm 2.58) \times 10^6 \text{ ns}^{-1}$  for  $\phi = 2.97$ . This indicates that water immersion rates decrease as the number of water molecules increases. The distinction of  $k_1$  for two adjacent  $N$  decreased with increasing  $N$ , which indicates that the number of water molecules should make no difference in water immersion when reaching a certain value. That is to say, the

number of water molecules is not an influence factor of water immersion at the macro level. It is relatively reasonable to choose the system of  $N = 39\,944$  to represent the practical situation. So, the mathematic model for water immersion curves with different aspect ratios will be built for the system of  $N = 39\,944$  in next section.

**Mathematic Model for Water Immersion Curves with Different Aspect Ratios.** To better fit the water immersion curves with different aspect ratios, especially for large  $N$ , a correction term is introduced into the Lucas–Washburn law, which is shown in the following equation

$$N_{in} = k_2 \sqrt{t} e^{-(\sqrt{t_0} / \sqrt{t})^b} \quad (3)$$

where  $e^{-(\sqrt{t_0} / \sqrt{t})^b}$  is the correction term and  $k_2$ ,  $t_0$ , and  $b$  are the fitting parameters. Here  $t_0$  is the function of aspect ratios and could indicate the time of the hysteresis in Stage I;  $k_2$  is the function of the dimension of the nanohole, surface tension, and viscosity and could indicate the water immersion rates for the whole process; and  $b$  is a power and considered as a constant. When  $t > t_0$ , the correction term approaches 1 and eq 3 is reduced to the Lucas–Washburn law.

**Figure 7** showed the time evolution of  $N_{in}$  for different aspect ratios for  $N = 39\,944$  at 300 K. All data were fitted by eq 3, and the fitted results are summarized in Table 3. The values of  $b$  are around  $1.65 \pm 0.15$  for different  $\phi$ . It is reasonable that the parameter  $b$  is considered to be a constant for multiple linear regression. The fitted curves and the value of  $R^2$  showed that the water immersion curves were all well-fitted, which indicates that eq 3 can express the water immersion process better in the actual situation. It could be found that the value of  $t_0^{1/2}$  decreased from 2.44 to 1.79 ns<sup>1/2</sup> with increasing  $\phi$ , which indicates that the time of the hysteresis in Stage I decreases with larger  $\phi$ . It was also clearly seen that  $k_2$  increased from 1103.11 to 1868.04 ns<sup>-1/2</sup> as aspect ratios increased, except  $\phi = 5.06$ . This indicates that water immersion rates increase with increasing  $\phi$  when  $\phi \leq 4.01$ . The increment of  $k_2$  for two adjacent  $\phi$  was 359.75, 315.57, 89.61, and

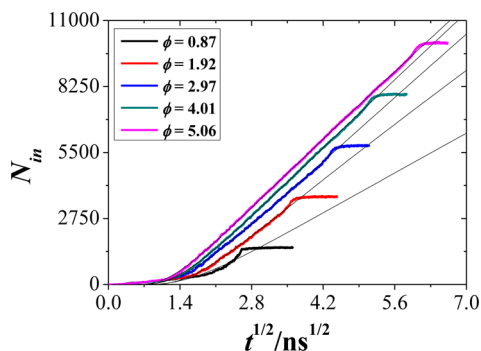


**Figure 7.** Time evolution of  $N_{in}$  for different aspect ratios for  $N = 39\,944$  at 300 K. The black solid curves showed the curves fitted by eq 3.

$-15.91 \text{ ns}^{-1/2}$ , respectively, from which it could be deduced that 4.01 is the best aspect ratio.

**Mechanism Analysis of Water Immersion Process.** The process of water immersion and its influence factors have been analyzed in detail; the mechanism of the water immersion process will be discussed in this section, which is mainly based on the above analysis. During the water immersion process, three kinds of driving forces play a key role in the different stages, which are the hydrogen bond in the bulk water, the interaction between water and silica, and the concentration gradient of water along the  $z$  axis. In Stage I, for the water molecules above the entrance of the nanohole, the hydrogen bond is dominant, so these water molecules move toward the bulk water. As the interaction between adsorbed water molecules and silica is enhanced, the water molecules gradually approach the entrance. Concentration gradients are more evident for higher aspect ratios, which contribute to water immersion. Therefore, the hysteresis weakens as aspect ratios increase. In Stage II, water molecules quickly move into the nanohole because the interaction of silanol groups on the hole surfaces and water molecules strengthens and the hydrogen bond for water molecules in the nanohole weakens. As the water molecules move downward, unwetted hole surfaces get smaller and smaller, which leads to a decline in the interaction between silica and water along the  $z$  axis. When the water molecules reach a certain depth, the hydrogen bond for water molecules in the nanohole no longer reduces. So the water molecules slowly immerse deeper in Stage III. Once the front of the meniscus reaches the bottom of the nanohole, the front wets the bottom first because of the strong interaction between silanol groups on the bottom surface and water molecules. The center is nearly still, which is due to the hydrogen bond between water molecules in the nanohole and the interaction of wetted silica and water molecules. Fast filling in Stage V is owing to the concentration gradient. The changes and balances between three kinds of driving forces determine the water immersion process.

## CONCLUSIONS

Our simulations demonstrated that the water immersion process into deep silica nanoholes could be divided into five stages. Higher aspect ratios are more beneficial for Stages I and II of water immersion. The water immersion process is determined by the changes and balances between three forms of driving forces: the hydrogen bond in the bulk water, the interaction between water and silica, and the concentration gradient of water along the  $z$  axis. Water immersion takes place more easily with higher aspect ratios ( $\phi$ ) and smaller numbers of water molecules ( $N$ ). The water immersion rates increase as the aspect ratios increase at the same  $N$ , but aspect ratios will make no difference in water immersion when reaching a certain value. Aspect ratios have a greater effect on water immersion rates for large  $N$ . For the same  $\phi$ , the rates decrease with larger  $N$ . A mathematic model is built to better express the water immersion with different aspect ratios in the practical application. This work on the effect of aspect ratios on water immersion could be meaningful for the micromachining process and other physical, biological processes.

## AUTHOR INFORMATION

### Corresponding Authors

\*Y.L.: E-mail: liuyingch@zju.edu.cn. Fax: +86 571 87951895.  
Tel: +86 571 87951895.

\*Q.W.: E-mail: qiwang@zju.edu.cn.

### Notes

The authors declare no competing financial interest.

## ACKNOWLEDGMENTS

This work was financially supported by the National Natural Science Foundation of China (nos. 21273200 and J1210042). We acknowledge Special Program for Applied Research on Super Computation of the NSFC-Guangdong Joint Fund (the second phase).

## REFERENCES

- (1) Topol, A. W.; Tulipe, D. C. L.; Shi, L.; Frank, D. J.; Bernstein, K.; Steen, S. E.; Kumar, A.; Singco, G. U.; Young, A. M.; Guarini, K. W.; Leong, M. Three-dimensional integrated circuits. *IBM J. Res. Dev.* **2006**, *50*, 491–506.
- (2) Graham, A. H. D.; Robbins, J.; Bowen, C. R.; Taylor, J. Commercialisation of CMOS Integrated Circuit Technology in Multi-Electrode Arrays for Neuroscience and Cell-Based Biosensors. *Sensors* **2011**, *11*, 4943–4971.
- (3) Bourg, I. C.; Steefel, C. I. Molecular Dynamics Simulations of Water Structure and Diffusion in Silica Nanopores. *J. Phys. Chem. C* **2012**, *116*, 11556–11564.
- (4) Leung, K.; Rempe, S. B.; Lorenz, C. D. Salt Permeation and Exclusion in Hydroxylated and Functionalized Silica Pores. *Phys. Rev. Lett.* **2006**, *96*, 095504.
- (5) Yamashita, K.; Daiguji, H. Molecular Dynamics Simulations of Water Uptake into a Silica Nanopore. *J. Phys. Chem. C* **2015**, *119*, 3012–3023.

**Table 3. Fitting Ranges and Fitted Parameters for the Water Immersion Curves for  $N = 39944$  by Equation 3<sup>a</sup>**

$N = 39\,944$	$[t_{start}^{1/2}, t_{end}^{1/2}] / \text{ns}^{1/2}$	$t_0^{1/2} / \text{ns}^{1/2}$	$k_2 / \text{ns}^{-1/2}$	$b$	$R^2$
$\phi = 0.87$	[0, 2.61]	2.44	1103.11	1.51	0.9266
$\phi = 1.92$	[0, 3.62]	2.31	1462.86	1.79	0.9966
$\phi = 2.97$	[0, 4.44]	2.17	1778.43	1.49	0.9993
$\phi = 4.01$	[0, 5.20]	2.04	1868.04	1.58	0.9997
$\phi = 5.06$	[0, 6.08]	1.79	1852.13	1.63	0.9998

<sup>a</sup> $R^2$  is corrected determination coefficient for the fitted curves.

- (6) Yamashita, K.; Daiguji, H. Molecular Simulations of Water Adsorbed on Mesoporous Silica Thin Films. *J. Phys. Chem. C* **2013**, *117*, 2084–2095.
- (7) Isaienko, O.; Borguet, E. Hydrophobicity of Hydroxylated Amorphous Fused Silica Surfaces. *Langmuir* **2013**, *29*, 7885–7895.
- (8) Musso, F.; Mignon, P.; Ugliengo, P.; Sodipe, M. Cooperative effects at water-crystalline silica interfaces strengthen surface silanol hydrogen bonding. An ab initio molecular dynamics study. *Phys. Chem. Chem. Phys.* **2012**, *14*, 10507–10514.
- (9) Bagherzadeh, S. A.; Englezos, P.; Alavi, S.; Ripmeester, J. A. Influence of Hydrated Silica Surfaces on Interfacial Water in the Presence of Clathrate Hydrate Forming Gases. *J. Phys. Chem. C* **2012**, *116*, 24907–24915.
- (10) Ho, T. A.; Argyris, D.; Papavassiliou, D. V.; Striolo, A.; Lee, L. L.; Cole, D. R. Interfacial water on crystalline silica: a comparative molecular dynamics simulation study. *Mol. Simul.* **2011**, *37*, 172–195.
- (11) Fogarty, J. C.; Aktulga, H. M.; Grama, A. Y.; van Duin, A. C. T.; Pandit, S. A. A reactive molecular dynamics simulation of the silica-water interface. *J. Chem. Phys.* **2010**, *132*, 174704.
- (12) Adeagbo, W. A.; Doltsinis, N. L.; Klevakina, K.; Renner, J. Transport Processes at  $\alpha$ -Quartz–Water Interfaces: Insights from First-Principles Molecular Dynamics Simulations. *ChemPhysChem* **2008**, *9*, 994–1002.
- (13) Lopes, P. E. M.; Murashov, V.; Tazi, M.; Demchuk, E.; MacKerell, A. D. Development of an Empirical Force Field for Silica. Application to the Quartz-Water Interface. *J. Phys. Chem. B* **2006**, *110*, 2782–2792.
- (14) Wensink, E. J. W.; Hoffmann, A. C.; Apol, M. E. F.; Berendsen, H. J. C. Properties of Adsorbed Water Layers and the Effect of Adsorbed Layers on Interparticle Forces by Liquid Bridging. *Langmuir* **2000**, *16*, 7392–7400.
- (15) Renou, R.; Szymczyk, A.; Ghoufi, A. Water confinement in nanoporous silica materials. *J. Chem. Phys.* **2014**, *140*, 044704.
- (16) Milischuk, A. A.; Ladanyi, B. M. Structure and dynamics of water confined in silica nanopores. *J. Chem. Phys.* **2011**, *135*, 174709.
- (17) Lerbret, A.; Lelong, G.; Mason, P. E.; Saboungi, M. L.; Brady, J. W. Water Confined in Cylindrical Pores: A Molecular Dynamics Study. *Food Biophys.* **2011**, *6*, 233–240.
- (18) Gallo, P.; Rovere, M.; Spohr, E. Glass transition and layering effects in confined water: A computer simulation study. *J. Chem. Phys.* **2000**, *113*, 11324–11335.
- (19) Stroberg, W.; Keten, S.; Liu, W. K. Hydrodynamics of Capillary Imbibition under Nanoconfinement. *Langmuir* **2012**, *28*, 14488–14495.
- (20) Bakli, C.; Chakraborty, S. Capillary filling dynamics of water in nanopores. *Appl. Phys. Lett.* **2012**, *101*, 153112.
- (21) Joly, L. Capillary filling with giant liquid/solid slip: Dynamics of water uptake by carbon nanotubes. *J. Chem. Phys.* **2011**, *135*, 214705.
- (22) Stukan, M. R.; Ligneul, P.; Crawshaw, J. P.; Boek, E. S. Spontaneous Imbibition in Nanopores of Different Roughness and Wettability. *Langmuir* **2010**, *26*, 13342–13352.
- (23) Ahadian, S.; Mizuseki, H.; Kawazoe, Y. On the kinetics of the capillary imbibition of a simple fluid through a designed nanochannel using the molecular dynamics simulation approach. *J. Colloid Interface Sci.* **2010**, *352*, 566–572.
- (24) Ahadian, S.; Kawazoe, Y. A molecular dynamics approach to examine the kinetics of the capillary imbibition of a polymer at nanoscale. *Colloid Polym. Sci.* **2009**, *287*, 961–967.
- (25) Dimitrov, D. I.; Milchev, A.; Binder, K. Molecular Dynamics Simulations of Capillary Rise Experiments in Nanotubes Coated with Polymer Brushes. *Langmuir* **2008**, *24*, 1232–1239.
- (26) Dimitrov, D.; Milchev, A.; Binder, K. Capillary Rise in Nanopores: Molecular Dynamics Evidence for the Lucas-Washburn Equation. *Phys. Rev. Lett.* **2007**, *99*, 054501.
- (27) Gruener, S.; Hofmann, T.; Wallacher, D.; Kityk, A. V.; Huber, P. Capillary rise of water in hydrophilic nanopores. *Phys. Rev. E* **2009**, *79*, 067301.
- (28) Gruener, S.; Huber, P. Spontaneous Imbibition Dynamics of an n-Alkane in Nanopores: Evidence of Meniscus Freezing and Monolayer Sticking. *Phys. Rev. Lett.* **2009**, *103*, 174501.
- (29) Gruener, S.; Huber, P. Imbibition in mesoporous silica: rheological concepts and experiments on water and a liquid crystal. *J. Phys.: Condens. Matter* **2011**, *23*, 184109.
- (30) Oh, J.; Faez, T.; de Beer, S.; Mugele, F. Capillarity-driven dynamics of water-alcohol mixtures in nanofluidic channels. *Microfluid. Nanofluid.* **2010**, *9*, 123–129.
- (31) Yang, W.; Fang, J.; Liu, P.; Li, J.; Cai, K. Theoretical study of the permeation of water through TiO<sub>2</sub> nanotubes using molecular dynamics simulation. *Mol. Phys.* **2011**, *109*, 969–974.
- (32) Guégan, R.; Morineau, D.; Alba-Simionescu, C. Interfacial structure of an H-bonding liquid confined into silica nanopore with surface silanols. *Chem. Phys.* **2005**, *317*, 236–244.
- (33) Zhuravlev, L. T. The surface chemistry of amorphous silica. Zhuravlev model. *Colloids Surf., A* **2000**, *173*, 1–38.
- (34) Berendsen, H. J. C.; van der Spoel, D.; van Drunen, R. GROMACS: A message-passing parallel molecular dynamics implementation. *Comput. Phys. Commun.* **1995**, *91*, 43–56.
- (35) Berendsen, H. J. C.; Grigera, J. R.; Straatsma, T. P. The missing term in effective pair potentials. *J. Phys. Chem.* **1987**, *91*, 6269–6271.
- (36) Hess, B.; Bekker, H.; Berendsen, H. J. C.; Fraaije, J. G. E. M. LINCS: A linear constraint solver for molecular simulations. *J. Comput. Chem.* **1997**, *18*, 1463–1472.
- (37) Hockney, R. W.; Goel, S. P.; Eastwood, J. W. Quiet high-resolution computer models of a plasma. *J. Comput. Phys.* **1974**, *14*, 148–158.
- (38) Bussi, G.; Donadio, D.; Parrinello, M. Canonical sampling through velocity rescaling. *J. Chem. Phys.* **2007**, *126*, 014101.
- (39) Essmann, U.; Perera, L.; Berkowitz, M. L.; Darden, T.; Lee, H.; Pedersen, L. G. A Smooth Particle Mesh Ewald Method. *J. Chem. Phys.* **1995**, *103*, 8577–8593.
- (40) Darden, T.; York, D.; Pedersen, L. Particle Mesh Ewald: An N-log(N) Method for Ewald Sums in Large Systems. *J. Chem. Phys.* **1993**, *98*, 10089–10092.
- (41) Washburn, E. W. The Dynamics of Capillary Flow. *Phys. Rev.* **1921**, *17*, 273.